Precision determination of the fine-structure interval in the ground state of positronium. IV. Measurement of positronium fine-structure density shifts in noble gases*

P. O. Egan, V. W. Hughes, and M. H. Yam
Gibbs Laboratory, Physics Department, Yale University, New Haven, Connecticut 06520
(Received 13 January 1976)

The fine-structure interval $\Delta\nu$ of ground state ($n = 1$) positronium has been measured to high precision, yielding $\Delta\nu = 203.3849(12)$ GHz (6 ppm). Comparison with theory is at present limited by uncalculated terms of order $\alpha^2\Delta\nu$. Values for the linear coefficient of the fine-structure density shift, $a \equiv (1/\Delta\nu)\partial\Delta\nu/\partial D$, have been measured for positronium in nitrogen and the noble gases: $a(N_2) = (-3.2 \pm 0.5) \times 10^{-5}$ atm^{-1} (0°C), a(He) $= (+1.6 \pm 0.3) \times 10^{-5}$ atm^{-1} (0°C), a(Ne) $= (-1.9 \pm 0.4) \times 10^{-5}$ atm^{-1} (0°C), a(Ar) $= (-6.2 \pm 0.3) \times 10^{-5}$ atm^{-1} (0°C), a(Kr) $= (-6.6 \pm 0.5) \times 10^{-5}$ atm^{-1}(0°C), and a(Xe) $= (-7.3 \pm 1.7) \times 10^{-5}$ atm^{-1} (0°C). The positronium density shifts differ markedly from those of hydrogen.

I. INTRODUCTION

The preceding article,[1] denoted paper III, described a measurement of the positronium ground-state fine-structure interval, $\Delta\nu$, to an accuracy of 20 parts per million (ppm). The present article, paper IV, reports an improved measurement of $\Delta\nu$ to a precision of 6 ppm, obtained with the same equipment as in paper III but with the addition of an on-line computer for control and data acquisition. Our experimental result provides a most sensitive test of quantum electrodynamics and of the Bethe-Salpeter equation.

The current experiment included a careful study of the dependence of $\Delta\nu$ on gas density for positronium formed in nitrogen. In addition, the density shifts of $\Delta\nu$ in the noble gases have been measured for the first time.

The original measurement of $\Delta\nu$ for positronium was made by Deutsch *et al.*[2] Earlier papers in the present series of precision measurements of $\Delta\nu$ are paper I by Hughes *et al.*,[3] paper II by Theriot *et al.*[4] and paper III by Carlson *et al.*[1] A recent measurement by Mills and Bearman[5] has reported $\Delta\nu$ to a precision of 8 ppm. Preliminary reports of the results of the present experiment have been published.[6,7]

II. THEORY OF THE EXPERIMENT

The major goal of this work is the comparison of the experimental value of $\Delta\nu$ with the value predicted by theory.[8,9,10,11] The current theoretical expression for $\Delta\nu$, ignoring all incompletely calculated orders in the expansion,[12,13,14] is

$$\Delta\nu = \tfrac{1}{2}\alpha^2\mathcal{R}c\left[\tfrac{7}{3} - (\alpha/\pi)\left(\tfrac{32}{9} + 2\ln 2\right) + \alpha^2\ln\alpha^{-1}\right] . \tag{1}$$

Using the values for α, $\mathcal{R}$, and c given in Eq. (1) of paper III, yields

$$\Delta\nu = 203.404\,117(86)\ \text{GHz}(0.42\ \text{ppm}) . \tag{2}$$

The uncertainty quoted in $\Delta\nu$ is due to the uncertainty of the fine-structure constant α, and does not take into account the uncalculated terms. A more reasonable estimate of the theoretical uncertainty is the order of the uncalculated terms, $\alpha^2\Delta\nu = 11$ MHz (50 ppm).

Some of the terms of order $\alpha^4\mathcal{R}c$ have recently been calculated by Fulton[15] and by Samuel.[16] These additional calculated terms are

$$-\tfrac{1}{2}\alpha^2\mathcal{R}c(\alpha/\pi)\left[\tfrac{1883}{288}\pi^2 - \tfrac{1303}{324} - \tfrac{37}{8}\zeta(3) - \tfrac{19}{12}\pi^2\ln 2\right] . \tag{3}$$

Inclusion of this contribution of Eq. (3) changes the theoretical value of Eq. (2) by 103 ppm to the value

$$\Delta\nu = 203.383\,267(86)\ \text{GHz}\ \ (0.42\ \text{ppm}). \tag{4}$$

However, the uncalculated terms still limit the theoretical precision to $O(\alpha^2\Delta\nu)$.

The theory of the line shape for the orthopositronium resonance transition has been derived in paper II. Our experiment measures the change in the 2γ decay mode induced by a transverse magnetic field, H_1, with an angular frequency, ω, near that of the Zeeman frequency, $\omega_{01} = 2\pi f_{01}$ [see Eq. (2) of paper III]. The 2γ decay signal can be calculated as in paper II and is found to be

$$S = \frac{\lambda_{10,2}}{4\lambda_{10}} + \left\{\frac{\lambda_{10,2}}{\lambda_{10}}(\lambda_0+\lambda_{10})\frac{V^2}{\hbar^2}\left(\frac{1}{2\lambda_0} - \frac{1}{\lambda_{10}}\right)\left[\frac{1}{(\omega-\omega_{01})^2 + \frac{1}{2}(\lambda_0+\lambda_{10}) + 2(\lambda_0+\lambda_{10})^2V^2/\lambda_{10}\lambda_0\hbar^2}\right]\right\} , \tag{5}$$

in which

$$V=\frac{xg'\mu_B H_1}{4[1+x^2+(1+x^2)^{1/2}]^{1/2}}\ .$$

x is the dimensionless static magnetic field index [Eq. (2), paper III], g' is the bound-state electron g factor [Eq. (3), paper III], and λ_0, λ_{10}, $\lambda_{10,2}$ are given by Eqs. (6) and (7) of Paper II. The assumptions made in the derivation of Eq. (5), which applies for a free positronium atom at rest are (1) phenomenological treatment of positronium annihilation, (2) neglect of initial positron polarization, and (3) neglect of off-resonant terms.

The fitting procedure of the present experiment did not use the simplifying approximations to the line shape described in Eq. (13) of paper III. Instead, the exact line shape, Eq. (5), was used throughout the data analysis. The line shape equation, (5), is cast in a considerably simpler form than the final line shape equations presented in paper II. The simplicity is the result of algebraic manipulation and does not reflect any basic change in the theory of the line shape.

III. EXPERIMENTAL APPARATUS

The apparatus used in this experiment was a refinement of the system used in paper III. The magnet, microwave system, and detectors are unchanged from paper III. The data-acquisition system in paper III was unable to handle high counting rates, because the multichannel analyzer used to scale coincidence counts had an appreciable dead time. Also the manual adjustments required during the sweep of the resonance line were too complicated to allow rapid acquisition of an experimental line shape, and hence the system was susceptible to long-term gain and timing drifts, which limited the precision of the data.

The present experiment surmounted these problems by automation of the data-acquisition system. A PDP 11/40 minicomputer[17] and associated CAMAC electronics were added to the system, and the resulting improvements in data-taking efficiency made a statistical improvement of the $\Delta\nu$ measurement possible.

A. Microwave system

A block diagram of the microwave electronics which produced magnetic fields of 10–20 G at 2.3 GHz in a TM110 cavity is shown in Fig. 1. The only addition to the system described in Part III was CAMAC control of the power leveling system, which allowed the microwave crystal voltage to be continuously monitored by the computer. The new system stabilized the crystal voltage to 0.03%.

B. Magnet system

The electromagnet and NMR system were essentially the same as in paper III, with additions made to allow automatic field sweep and NMR lock by the computer. A diagram of the system is shown in Fig. 2.

The NMR frequency was automatically set by a CAMAC-controlled frequency synthesizer,[18] and the magnet Fieldial regulator[19] controls were coupled to stepping switches and motors so that the magnetic field could be set and swept by the computer. The NMR receiver was modified by the addition of a discriminator which provided T^2L levels to indicate whether the field was on or off NMR lock, which in turn were used to generate computer interrupts. In operation the desired sequence of NMR frequencies, which constituted an experimental field sweep, was entered into the computer at the start of the experiment. The program then adjusted the magnet regulator to lock the NMR system at the desired frequencies in succession.

The magnetic field distribution over the positronium observation region was mapped as de-

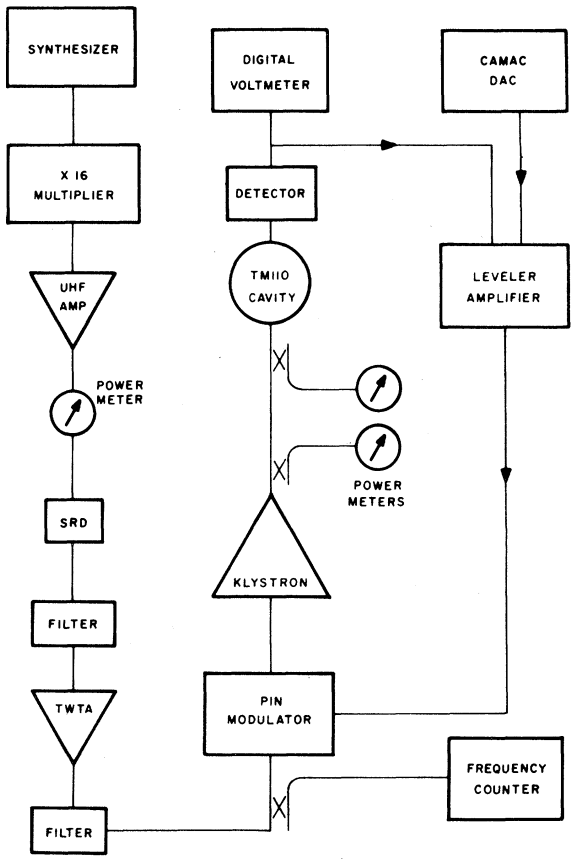

FIG. 1. Block diagram of microwave system.

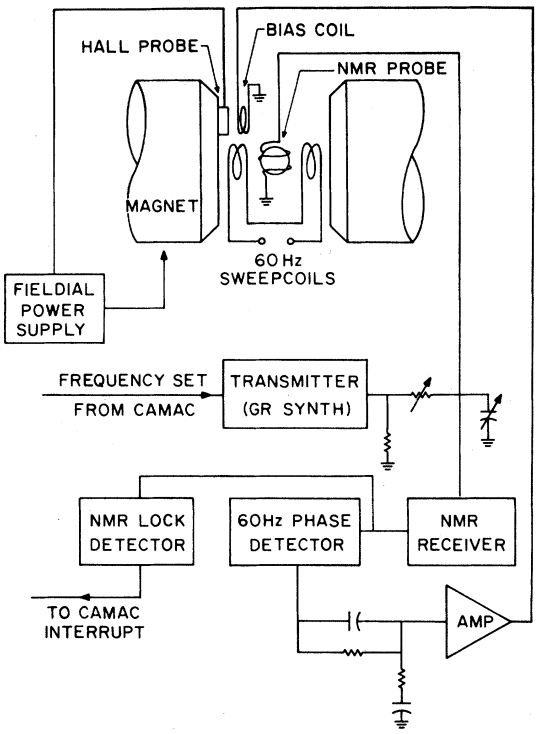

FIG. 2. Block diagram of NMR magnet regulation system.

scribed in paper III, and no significant change from the previous measurement was seen. The rms field distribution over the observation region was measured to be 1.2 ppm.

A critical parameter in this experiment is the difference between the NMR frequency measured by the mineral oil probe located in the cavity lid and the NMR frequency for a standard sample (spherical H_2O) at the positronium observation region (center of cavity). The factors which contribute to this frequency difference are (1) the NMR frequency at the center of the cavity was measured to be 4.6 ± 0.7 ppm lower than that at the lid position, (2) the NMR frequency for protons in mineral oil is 3.7 ± 0.6 ppm lower than that for protons in water,[1,20] and (3) our NMR probe is found to be equivalent (to within 0.5 ppm) to a cylindrical mineral oil sample. Protons in a cylindrical oil sample are known[20,21] to have an NMR frequency $\frac{2}{3}\pi|\chi(\text{oil})| = 1.5$ ppm higher than a spherical sample due to bulk diamagnetic shielding. Combining these three effects we conclude that the measured NMR frequency is 2.4 ± 1.0 ppm higher than that for a spherical H_2O sample at the cavity center.

C. Positron source

The positron source for our experiment was 5–10 mCi of Na^{22}, two to four times as intense as the source used in paper III. The source mounting assembly was identical to the previous measurement.

D. Gas-handling system

The main improvement in the gas-handling system was substitution of a 25-l/sec ion pump[22] in place of the oil-diffusion pump, and a cryogenic sorption pump in place of the mechanical pump, to improve system cleanliness.

E. Detectors

The only modification to the γ-ray detection apparatus of paper III was the inclusion of computer-controlled high-voltage DACs to control automatically the photomultiplier gains. The HV DACs function as part of a computer-controlled automatic gain-control system.

The detector geometry consists of four pairs of NaI detectors to monitor the 2γ rate, as described in paper III.

F. Fast electronics

The photomultiplier pulses were processed by fast pulse electronics to yield the 2γ counts. The singal processing requirements were as follows: (1) Each photopulse must have height consistent with that of a 511-keV γ ray before it is accepted as a single γ event. (2) A 2γ signal is formed by coincidence gating 1γ signals from two collinear detectors on opposite sides of the cavity. Thus both detected gamma rays must have energy and momentum consistent with 2γ annihilation. (3) The 2γ signal must be scaled. (4) The photopeak spectra of the individual PMTs must be routed to the computer for pulse-height analysis and automatic gain control.

Figure 3 shows the electronics used to meet these requirements for a single detector pair. The positive preamp pulses were energy analyzed by timing single-channel analyzers (TSCAs). The upper and lower discriminators of the TSCAs were set to define an energy window for the 0.51-MeV photopeak. The analyzer gave an output pulse only for detected gammas with the correct energy. The TSCA output pulses were lengthened to 100 nsec by univibrators to fix the coincidence resolving time at 200 nsec. The 100-nsec 1γ pulses were coincidence gated in collinear pairs and the coincident 2γ output pulse was lengthened by a uni to provide a 1.5-μsec gating pulse for the pulse-height analysis logic. The 2γ gate-generator outputs were counted by CAMAC scalers. The computer inhibits the scalers from counting when it senses that one of the experimental parameters, e.g., the magnetic field, is out of line.

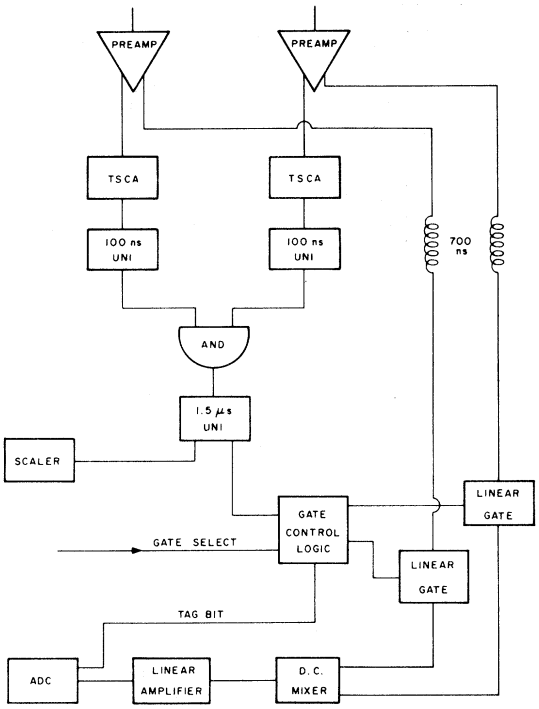

FIG. 3. Logic diagram of coincidence detection circuit.

The time reference for the scaler rates is a 1-MHz signal derived from the local frequency standard which is scaled by a 48-bit CAMAC scalar enabled and inhibited simultaneously with the 2γ scalers.

The pulse-height analysis logic was designed so that two PMT outputs at a time could be designated by the computer to be sampled by an ADC. The negative preamplifier pulses were delayed by RG 58C/U cable to match the time delay of the coincidence logic and then input to linear gates. The gating logic allowed the analog outputs of two detectors from different coincidence pairs to be selected by the computer for analysis. The two preselected detectors are then gated by 2γ pulses from the coincidence logic. A tag bit to identify the coincident pair from which the analog signal originates is generated by the gating logic.

The linear gate outputs are combined in dc mixers, amplified and inverted, and the resulting pulse heights are digitized by an analog-to-digital converter (ADC). The ADC, along with the identifying tag bit from the logic module is read by a Yale CAMAC-ADC interface. The digital pulse-height information is used to increment a corresponding word of the computer memory, so that a pulse-height spectrum is accumulated for further analysis.

The counting rates of the coincidence circuits depended on the pressure. Typical 2γ coincidence rates for a detector pair varied from 500 counts/sec to 2000 counts/sec over the range of experimental conditions. Typical 1γ counting rates were 10 000–20 000 counts/sec.

G. Computer control hardware

The automation and control of the experiment by the computer was a critical factor in improving the ultimate accuracy. The devices tied to the computer CPU consist of a Decwriter, a display terminal, and a papertape reader/punch. A Yale CAMAC Branch Driver interfaces the computer bus to the CAMAC Dataway. A programmable real-time clock is used to generate interrupts.

The CAMAC configuration used is shown in Fig. 4. The functions of the individual modules are as follows:

i. Scalers. Yale 300 MHz dual scalers count the 2γ coincidences and the 1-MHz time reference. The scaler crate is cleared and enabled when data are ready to be taken at a field point, and inhibited when the computer senses that the NMR lock is off or the microwave crystal detector voltage is away from its preset range. Enables and inhibits occur simultaneously for all scalers. At the end of a field point the scalers are read and output.

ii. NMR frequency control. The frequency of the NMR synthesizer is set by a register which drives the external BCD frequency input of the synthesizer.

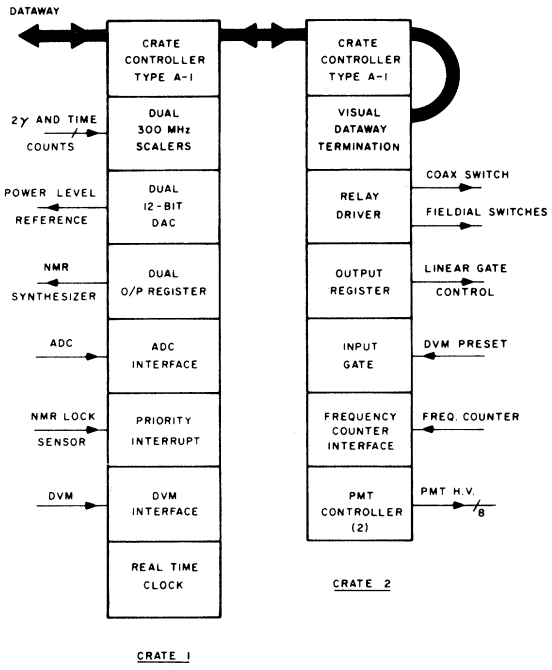

FIG. 4. Block diagram of CAMAC system.

iii. NMR field-lock interrupts. The NMR lock "on/off" signals from the NMR lock detector described in Sec. III B enter a CAMAC interrupt module and generate computer interrupts when the field-lock status changes.

iv. Relay driver. A CAMAC driver is used to step the Fieldial stepping switches and stepping motor and to drive the coax switch which multiplexes the inputs to the frequency counter.

v. Frequency counter interface. A Yale frequency counter interface was specially designed to read the BCD output of a frequency counter. Both microwave and NMR frequencies are read.

vi. DVM preset. The preset value for the microwave crystal voltage is set by Digiswitches which are read by a CAMAC input gate.

vii. DVM interface. A Yale DVM interface was designed to read the DVM. The microwave crystal voltage is continually sampled by the DVM and compared with its preset value.

viii. Power leveling DAC. The power adjustment routine alters the output voltage of a 12-bit DAC to adjust the reference level of the microwave leveller amplifier and bring the crystal voltage back to its preset value.

ix. Linear gate control. An output register supplies the 4-bit gate select signal to the linear gate controller described in Sec. III F.

x. ADC interface. A Yale ADC Interface reads the ADC. The accumulated pulse-height spectra are crudely analyzed on-line to determine the approximate line center. Gain drifts which cause a shift in the line center may then be corrected by adjusting the PMT high voltage.

H. Experimental procedure and computer software

Preparatory to a data run, the cavity was pumped to a pressure of 10^{-5} Torr and filled with high-purity gas. The magnet, microwave system, and counting electronics were warmed up and checked during this period. When the warm-up procedure was completed, the positronium data acquisition program was started. A simplified flowchart of the program is shown in Fig. 5.

In the initial states of the program all device interrupts and internal flags are set and the run identification number, the number of field points in a pass, the Fieldial switch settings and NMR frequencies for a pass sequence, and the running time for an individual field point are input on the Decwriter. The field sequence was the same for all runs and consists of an upward and a downward sweep over a 400-G range centered on the approximate resonance magnetic field at 7.8 kG. The run time at each field point was preset at approximately four minutes, and a complete pass

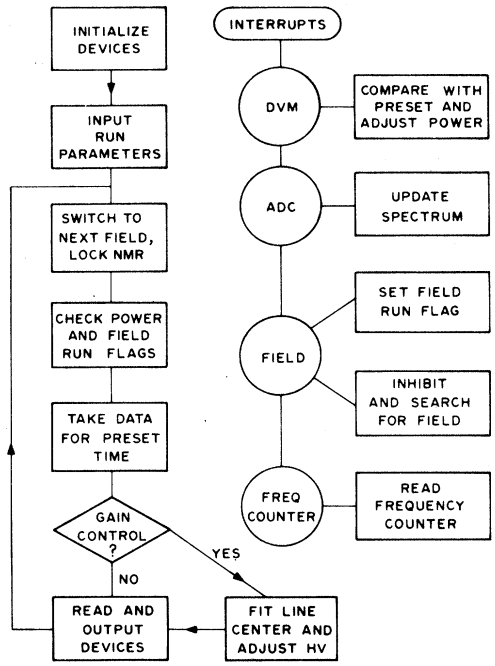

FIG. 5. Simplified flowchart of data acquisition program.

sequence took ~1.5 h.

To take data at a given field point, the NMR frequency and Fieldial switch positions are first set by the computer. The Fieldial range dial is then searched until NMR field lock is achieved. Meanwhile the microwave crystal voltage is compared with its preset value, and when both microwave power and magnetic field are ready the data-taking commences. During the data-taking period the program may be interrupted by a "field-off" signal, a DVM interrupt, or an ADC interrupt (if the gain-control program is enabled).

When the internal clock has counted for the preset four minutes, the data acquisition is halted. If the gain-control routine is in operation, the approximate line centers of the photopeak spectra are determined by fitting the accumulated peaks to a triangular function and adjustments of the PMT voltages are made if needed. The CAMAC 2γ and time scalers are read, along with the microwave and NMR frequencies. Data and time of day information are read from the CAMAC real time clock.

The data are output on paper tape in ASCII format. Each paper tape record consists of the run identification number, the pass number, the date and time of day, the microwave frequency, the NMR frequency, the 2γ scaler counts, and the time scaler counts. The scaler counts are also printed on the Decwriter.

After the data output is complete, the program returns to the field setting routine for the next point in the pass cycle.

Each run at a given pressure consists of 15 to 45 consecutive passes and represents from one to three days of continuous data taking.

IV. ANALYSIS OF DATA

The experimental 2γ coincidence counts versus magnetic field yields the orthopositronium Zeeman resonance signal, which must be fit with the theoretical line shape of Eq. (5).

At a fixed microwave frequency, ω, and a given magnetic field, the signal S depends on two parameters: $\Delta\nu$ and H_1. At a given field point the NMR frequency at the center of the cavity for protons in a spherical water sample, f_p, is known from the measured NMR frequency modified by the offset and shielding corrections given in Sec. III B.

In the actual fitting routine $\Delta\nu$ is not used as the free parameter, instead the program fits to find f_p^c, the NMR frequency at the line center ($\omega = \omega_{01}$), which is related to $\Delta\nu$ by

$$\Delta\nu = \left(\frac{g'}{2(\mu_p'/\mu_B)}\right)^2 \frac{(f_p^c)^2}{f_{01}} - f_{01} \ , \qquad (6)$$

[Eq. (16) of paper III]. The quantity μ_p'/μ_B is the proton magnetic moment in Bohr magnetons for a spherical water sample[23] [$\mu_p'/\mu_B = 1.520\,992\,983\ (17) \times 10^{-3}$], and f_{01} is the microwave frequency.

The experimental data are fit to the expression for the line shape given in Eq. (15) of paper III, where S is now taken as the exact expression of Eq. (5). A more general polynomial expression for the background was also used, but gave no improvement in fit compared to the linear background fit.

A typical fitted line shape is shown in Fig. 6.

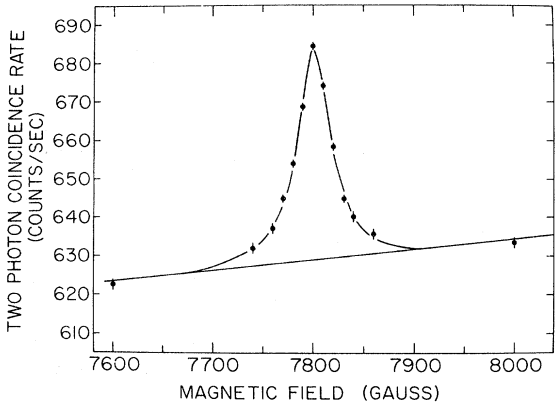

FIG. 6. Typical data for a resonance pass fit to the theoretical lineshape. $f_{01} = 2323.364$ MHz, 0.31 atm N_2.

TABLE I. Fitted values of $\Delta\nu$ for each run.

N_2 density (atm) 0 °C	H_1 (G)	$\Delta\nu$ (GHz)	σ (GHz)
0.251	13.2	203.3807	0.0046
0.251	12.6	203.3831	0.0022
0.314	13.5	203.3864	0.0023
0.314	14.1	203.3825	0.0018
0.377	16.5	203.3815	0.0016
0.439	13.1	203.3831	0.0025
0.565	16.8	203.3833	0.0026
0.628	16.5	203.3782	0.0020
0.941	19.7	203.3785	0.0020
1.26	18.2	203.3817	0.0040
1.88	19.4	203.3719	0.0066
1.88	17.2	203.3683	0.0041
2.51	19.4	203.3665	0.0048
2.82	19.0	203.3680	0.0029

The points are the measured counting rates and are shown with one standard deviation error bars. The solid line is the best fit to the data obtained from the least square optimization routine. The presence of the field-dependent background is obvious in the fit. The data of Fig. 6 are the result of a one 1.5 h pass through the resonance for one detector pair.

A. Precision $\Delta\nu$ measurement in nitrogen

Nitrogen was used as the stopping gas for the precision $\Delta\nu$ measurement because its microwave breakdown properties allow data to be taken at low densities, as discussed in paper III. The measured values of $\Delta\nu$ and the standard deviations for each run at a given nitrogen density are tabulated in Table I and plotted in Fig. 7.

The measured $\Delta\nu$ values were fit to a linear density shift equation [Eq. (17) of paper III] as

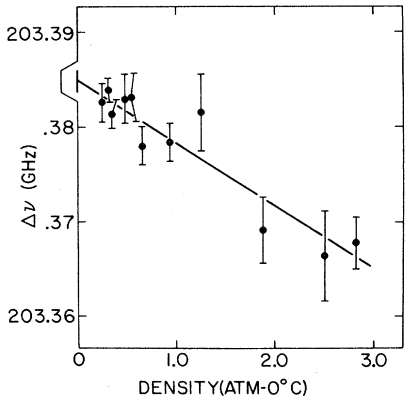

FIG. 7. Measured values of $\Delta\nu$ vs nitrogen density. The straight line is the best fit to a linear density dependence.

described in the previous section, giving

$$\Delta\nu(0) = 203.3849(10)\ \text{GHz}\ , \qquad (7)$$

where the error is the statistical counting error. The fitted value of the linear fractional density shift in nitrogen is

$$a(N_2)_{\text{lin}} = (-3.2 \pm 0.5) \times 10^{-5}\ \text{atm}^{-1}(0\,^\circ\text{C})\ . \qquad (8)$$

The linear fit is shown in Fig. 7.

The results of a fit of the data to a quadratic density shift equation [Eq. (18) of paper III] are displayed in Table II, together with the results of the linear fit. No evidence for a quadratic density dependence is indicated, and the linear fit is adopted for all further analysis.

A summary of the systematic contributions to the error in $\Delta\nu$ is shown in Table III. With regard to the basic assumptions underlying the derivation of the theoretical line shape of Eq. (5), the phenomenological treatment of positronium annihilation has not been justified fully theoretically, but, as in the case of the theoretical line shape for Lamb shift measurements in hydrogen,[24] it is expected to be sufficiently accurate. The errors associated with the other two assumptions of neglect of initial positron polarization and neglect of off-resonant terms are estimated in Table III to be very small. Apart from the density shift in $\Delta\nu$ due to collisions of positronium with gas molecules, there can also be a density shift in the effective g' value of positronium, as has been observed and calculated for other atoms.[25,26] This effect should be negligible for our positronium Zeeman transition, especially because only a quadratic Zeeman effect for the $M=0$ state is present. Other effects of collisions on the line shape have been discussed in papers I and II, and should not lead to any errors in the determination of $\Delta\nu$. We note from Table III that the dominant systematic errors are associated with our knowledge of the magnetic field H_0. When the systematic error of 3.3 ppm is combined with 1.0-MHz or 5.0-ppm statistical uncertainty in $\Delta\nu$ of Eq. (7), the total uncertainty is 1.2 MHz or 6 ppm. Thus the final value for $\Delta\nu$ obtained from this experiment is

$$\Delta\nu = 203.3849(12)\ \text{GHz}\ (6.0\ \text{ppm})\ . \qquad (9)$$

TABLE II. Results of density-dependent fits to the data of Table I.

Quantity	Linear fit	Quadratic fit
$\Delta\nu(0)$ (GHz)	203.3849 (10)	203.3856 (18)
a [10^{-5} atm^{-1}(0 °C)]	-3.2 ± 0.5	-4.1 ± 2.0
b [10^{-5} atm^{-2}(0 °C)]	0	0.3 ± 0.7
χ^2/degree of freedom	6.5/9	6.3/8

TABLE III. Summary of uncertainties in the measurement of $\Delta\nu$ (in ppm).

Counting statistics	5.0
Magnetic field inhomogeneity	2.4
Magnetic field offset and reproducibility	1.4
NMR probe susceptibility and shielding corrections	1.6
Microwave power instability	0.5
Density uncertainty	0.3
Microwave frequency uncertainty	0.1
Neglect of positron polarization in Eq. (5) [a]	0.2
Neglect of off-resonant terms in Eq. (5) [a]	0.4
Quadrature sum of uncertainties	6.0

[a] See paper II (Ref. 4).

The indicated error is 1/1200 of the natural linewidth.

B. Measurement of density shifts for positronium in noble gases

The values of $\Delta\nu$ measured for various noble-gas densities are shown in Table IV, along with the one-standard deviation errors. Special treatment is required for the case of argon and neon, where small fractions (5–10 %) of N_2 were added to the gas to avoid microwave breakdown. The $\Delta\nu$ values given in Table IV are those for the pure gas, obtained from the value measured for the mixture by subtracting the N_2 density shift, Eq. (8). The Ar and Ne densities in Table IV are the densities of the noble-gas fractions. The data of Table IV were fit both by allowing $\Delta\nu(0)$ to be a free parameter, and by constraining it to the nitrogen value of Eq. (9). The results of linear

TABLE IV. Measured values of $\Delta\nu$ in noble gases.

Stopping gas	Density (atm) 0 °C	$\Delta\nu$ (GHz)	σ (GHz)
He	1.88	203.3917	0.0021
	2.32	203.3945	0.0022
	2.82	203.3931	0.0015
Ne	1.26	203.3786	0.0018
	1.88	203.3945	0.0022
	2.82	203.3931	0.0015
Ar	1.13	203.3685	0.0016
	1.75	203.3615	0.0019
	2.69	203.3519	0.0020
Kr	1.26	203.3675	0.0021
	1.89	203.3597	0.0026
	2.84	203.3469	0.0035
Xe	0.626	203.3766	0.0050
	0.940	203.3710	0.0053
	1.26	203.3659	0.0054

TABLE V. (A) Linear-density shift fits to noble gas data with nitrogen $\Delta\nu(0)$ value as zero-density data point. $a \equiv (1/\Delta\nu)(\partial\Delta\nu/\partial D)$. (B) Linear-density shift fits to noble-gas data alone. $a \equiv (1/\Delta\nu)(\partial\Delta\nu/\partial D)$.

	Part A		Part B	
Gas	a (atm^{-1} 0 °C)	χ^2(fit)/d.f.	$\Delta\nu(0)$ (GHz)	a (atm^{-1} 0 °C)
He	$(1.6\pm0.3)\times10^{-5}$	1.4/2	203.3908(64)	$(0.4\pm1.2)\times10^{-5}$
Ne	$(-1.9\pm0.4)\times10^{-5}$	0.70/2	203.3819(36)	$(-1.2\pm0.9)\times10^{-5}$
Ar	$(-6.2\pm0.3)\times10^{-5}$	1.9/2	203.3804(30)	$(-5.2\pm0.8)\times10^{-5}$
Kr	$(-6.6\pm0.5)\times10^{-5}$	0.06/2	203.3839(47)	$(-6.4\pm1.2)\times10^{-5}$
Xe	$(-7.3\pm1.7)\times10^{-5}$	0.04/2	203.387(11)	$(-8.4\pm5.7)\times10^{-5}$

density shift fits to the noble-gas data for both fitting methods are displayed in Table V.

The values for $\Delta\nu(0)$ from the noble-gas data alone, Table VB, differ by no more than 1.5 standard deviations from the nitrogen value of Eq. (9). The nitrogen $\Delta\nu(0)$ value is therefore statistically consistent with the $\Delta\nu(0)$ values from the noble gases alone, and it can be used as the zero-density point in determining the density-shift coefficients of the noble gases. The values for the noble-gas density-shift coefficients determined by this experiment are the values given in Table VA.

The noble-gas $\Delta\nu$ data and the linear fit of Table VA are shown in Fig. 8. The data were also fit with quadratic density-shift formulas. No significant quadratic dependence was obtained. The noble-gas $\Delta\nu(0)$ values are not included in the final results for $\Delta\nu$.

V. SUMMARY

The principal result of this experiment was the measurement of the fine-structure interval of positronium in the ground state,

$$\Delta\nu_{\text{expt}} = 203.3849(12)\ \text{GHz}\ (6\ \text{ppm})\ . \qquad (10)$$

The linear fine-structure density shift in nitrogen was measured to be

$$a(N_2) \equiv (1/\Delta\nu)(\partial\Delta\nu/\partial D) = (-3.2\pm0.5)\times10^{-5}\ \text{atm}^{-1}\ (0\,^\circ\text{C})\ . \qquad (11)$$

A quadratic density dependence of $\Delta\nu$ in nitrogen was not observed.

The linear fine-structure density shifts for positronium in the noble gases were measured to be

$$\begin{aligned} a(\text{He}) &= (+1.6\pm0.3)\times10^{-5}\ \text{atm}^{-1}\ (0\,^\circ\text{C})\ , \\ a(\text{Ne}) &= (-1.9\pm0.4)\times10^{-5}\ \text{atm}^{-1}\ (0\,^\circ\text{C})\ , \\ a(\text{Ar}) &= (-6.2\pm0.3)\times10^{-5}\ \text{atm}^{-1}\ (0\,^\circ\text{C})\ , \\ a(\text{Kr}) &= (-6.6\pm0.5)\times10^{-5}\ \text{atm}^{-1}\ (0\,^\circ\text{C})\ , \\ a(\text{Xe}) &= (-7.3\pm1.7)\times10^{-5}\ \text{atm}^{-1}\ (0\,^\circ\text{C})\ . \end{aligned} \qquad (12)$$

A summary of this and all previous $\Delta\nu$ measurements is given in Table VI.

Ignoring all terms of order $\alpha^4\mathcal{R}c$ in the theory, the theoretical value is that of Eq. (2), $\Delta\nu_{\text{theor}} = 203.404\ 12(9)$ GHz, and the difference between the theoretical value and the results of this experiment is significant:

$$\Delta\nu_{\text{theor}} - \Delta\nu_{\text{expt}} = 19.1(1.2)\ \text{MHz}. \qquad (13)$$

If the partial calculation of the order $\alpha^4\mathcal{R}c$ terms is included, the theoretical value is given by Eq. (4), $\Delta\nu_{\text{theor}} = 203.383\ 27(9)$ GHz and the theoretical value is in agreement with experiment

$$\Delta\nu_{\text{theor}} - \Delta\nu_{\text{expt}} = 1.6(1.2)\ \text{MHz}\ . \qquad (14)$$

Clearly, a complete calculation of the next order in the theory is needed for comparison with experiment. The uncalculated terms of order $(\alpha^4\mathcal{R}c)$ are recoil and retardation terms characteristic of the two-body problem.

The positronium–noble-gas density shifts mea-

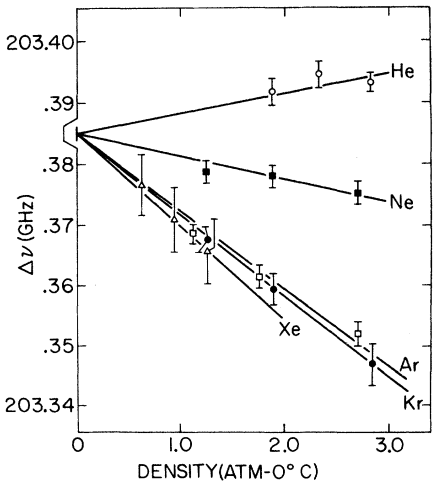

FIG. 8. Measured values of $\Delta\nu$ vs noble gas density (○—He; ■—Ne; □—Ar; ●—Kr; △—Xe). The straight lines show the best linear fits to the data including the value of $\Delta\nu(0)$ determined in N_2.

TABLE VI. Summary of precision measurements of positronium $\Delta\nu$.

$\Delta\nu$ (GHz)	Reference
203.380(40) (200 ppm)	Deutsch *et al.*[a]
203.330(40) (200 ppm)	Hughes *et al.*[b] (paper I)
203.403(12) (60 ppm)	Theriot *et al.*[c] (paper II)
203.384(4) (20 ppm)	Carlson *et al.*[d] (paper III)
203.3870(16) (8 ppm)	Mills and Bearman[e]
203.3849(12) (6 ppm)	This work (paper IV)

[a] Reference 2.
[b] Reference 3.
[c] Reference 4, without bound-state g-factor correction.
[d] Reference 1, linear density fit.
[e] Reference 5.

TABLE VII. Measured values for fractional density shifts of positronium and hydrogen in noble gases. $a \equiv (\Delta\nu)^{-1}\,(\partial\Delta\nu/\partial D)$.

Buffer gas	a (positronium) [atm^{-1} (0 °C)]	a (hydrogen) [atm^{-1} (0 °C)]
He	$+1.6(3)\times10^{-5}$	$+3.65(7)\times10^{-6}$ [a]
Ne	$-1.9(4)\times10^{-5}$	$+2.19(4)\times10^{-6}$ [a]
Ar	$-6.2(3)\times10^{-5}$	$-3.648(5)\times10^{-6}$ [b]
Kr	$-6.6(5)\times10^{-5}$	$-7.9(2)\times10^{-6}$ [c]
Xe	$-7.3(1.7)\times10^{-5}$	$-15(2)\times10^{-6}$ [c]

[a] Reference 27.
[b] Reference 29.
[c] Reference 28.

sured in this experiment are compared with the hydrogen hyperfine structure density shifts for the noble gases[27,28,29] in Table VII. From the table several striking differences are apparent between the positronium and hydrogen $\Delta\nu$ density shifts in the noble gases:

(i) The positronium density shifts are typically an order of magnitude larger than those of hydrogen.

(ii) The positronium–noble-gas density shift changes sign as the mass of the noble-gas atom increases; the helium shift is positive while the heavier atoms cause a negative shift. The sign change of the shift also occurs in hydrogen and is explained by the competition of long-range attractive and short-range repulsive forces in the collision process.[30] Note however, that the sign change occurs at a different place in the periodic table for the hydrogen and positronium cases; the density shift of hydrogen in neon is positive, while that of positronium in neon is negative.

(iii) The positronium density shifts in argon, kyrpton, and xenon have nearly the same value. This is quite different from the behavior of the heavy noble-gas density shifts for hydrogen where the shift increases by approximately a factor of 2 from Ar to Kr and from Kr to Xe.

A calculation[31] of hfs density shifts for positronium in noble gases, using atomic polarizabilities and a quantum mechanical thermal averaging, gives values agreeing within a factor of two with our experimental results, except for the case of He where the calculated value has the opposite sign to the measured value.

Since the limitation on the final value of $\Delta\nu$ of Eq. (10) in this experiment is still dominantly that imposed by counting statistics (see Table III), and the theoretical understanding of the line shape is not yet a limiting factor, further improvement in precision should be possible in our experiment. It seems practical to increase the counting rate by a factor of about 4 to 5 by increase in radioactive source strength and in detector solid angle. The systematic errors associated with the magnetic field can be reduced by improvements in the measurement of the magnetic field and of the positron stopping distribution.

The use of line-narrowing techniques,[32] may be applicable to improve the precision of the measurement of $\Delta\nu$, such as have been used for hydrogen fine structure[33] and muonium hfs[34,35] measurements.

ACKNOWLEDGMENTS

It is a pleasure to acknowledge the important contributions of Dr. E. R. Carlson to the early phases of this experiment, Mr. S. Dhawan to the development of the on-line computer system, Mr. W. E. Frieze assisted in the data-taking and Ms. S. Rothberg assisted with the data analysis.

*Research supported in part by the National Science Foundation (Grant No. GP 43847X).

[1] E. R. Carlson, V. W. Hughes, and I. Lindgren (preceding article). (paper III), Phys. Rev. A 15, 241 (1977).
[2] M. Deutsch and S. C. Brown, Phys. Rev. 85, 1047 (1952): R. Weinstein, M. Deutsch, and S. Brown, *ibid.* 94, 758 (1954); 98, 223 (1955).
[3] V. W. Hughes, S. Marder, and C. S. Wu, Phys. Rev. 106, 934 (1957) (paper I).
[4] E. D. Theriot, Jr., R. H. Beers, V. W. Hughes, and K. O. H. Ziock, Phys. Rev. A 2, 707 (1970) (paper II).
[5] A. P. Mills, Jr. and G. H. Bearman, Phys. Rev. Lett. 34, 246 (1975).
[6] P. O. Egan, E. R. Carlson, V. W. Hughes, and M. Yam,

Bull. Am. Phys. Soc. 20, 703 (1975). The preliminary result reported here was in error due to a computer error .
[7]P. O. Egan, W. E. Frieze, V. W. Hughes, and M. H. Yam, Phys. Lett. 54A, 412 (1975).
[8]S. J. Brodsky and S. D. Drell, Ann. Rev. Nucl. Sci. 20, 147 (1970).
[9]B. E. Lautrup, A. Peterman, and E. deRafael, Phys. Reports 3, 193 (1972).
[10]V. W. Hughes, in *Atomic Physics III*, edited by S. J. Smith and G. K. Walters (Plenum, New York, 1973), p. 1.
[11]V. W. Hughes, *Physik 1973*, German Physical Society Conference (Physik Verlag, Germany, 1973), p. 123.
[12]T. Fulton, D. A. Owen, and W. W. Repko, Phys. Rev. A 4, 1802 (1971).
[13]D. A. Owen, Phys. Rev. Lett. 30, 887 (1973).
[14]R. Barbieri, P. Christillin, and E. Remiddi, Phys. Rev. A 8, 2266 (1973).
[15]T. Fulton, Phys. Rev. A 7, 377 (1973).
[16]M. A. Samuel, Phys. Rev. A 10, 1450 (1974); M. A. Samuel, Research Note 52, Quantum Theoretical Research Group, Oklahoma State University (unpublished).
[17]Digital Equipment Corp.
[18]General Radio Model 1061.
[19]Varian Mark II.
[20]B. N. Taylor, W. H. Parker, and D. N. Langenberg, Rev. Mod. Phys. 41, 375 (1969).
[21]E. R. Andrew, *Nuclear Magnetic Resonance* (Cambridge U. P., Cambridge, 1955).
[22]Ultek Model 202-2500.
[23]W. D. Phillips, W. E. Cooke, and D. Kleppner, Phys. Rev. Lett. 35, 1619 (1975).
[24]F. E. Low, Phys. Rev. 88, 53 (1952).
[25]J. Jarecki and R. M. Herman, Phys. Rev. Lett. 28, 199 (1972).
[26]J. S. Tiedman and H. G. Robinson, in *Atomic Physics III*, edited by S. J. Smith and G. K. Walters (Plenum, New York, 1973), p. 85.
[27]F. M. Pipkin and R. H. Lambert, Phys. Rev. 127, 787 (1962).
[28]E. S. Ensberg and C. L. Morgan, Phys. Lett. 28A, 106 (1968).
[29]C. L. Morgan and E. S. Ensberg, Phys. Rev. A 7, 1494 (1968).
[30]B. K. Rao, D. Ikenberry and T. P. Das, Phys. Rev. A 2, 1411 (1970).
[31]G. H. Bearman and A. P. Mills, Jr., Phys. Lett. 56A, 350 (1976).
[32]V. W. Hughes, *Quantum Electronics*, edited by C. H. Townes (Columbia U. P., New York, 1960).
[33]C. W. Fabjan and F. M. Pipkin, Phys. Rev. A 6, 556 (1972).
[34]D. Favart *et al.*, Phys. Rev. A 8, 1195 (1973).
[35]D. Casperson *et al.*, Phys. Lett. 59B, 397 (1975).